Clays and Clay Minerals, Vol. 67, No. 6:461–470, 2019

SYNTHESIS, STRUCTURE, AND FERROELECTRICITY OF A KAOLINITE-*p*–AMINOBENZAMIDE INTERCALATION COMPOUND

Shun-Ping Zhao[1] *, Yu Guo[2], Miao-Miao Zhu[1], Jie Wang[1], Xiao-Liang Feng[1], Qiao Qiao[3], and Heng Xu[1]

[1]Anhui Key Laboratory of Photoelectric-Magnetic Functional Materials, Anhui Key Laboratory of Functional Coordination Compounds, School of Chemistry and Chemical Engineering, Anqing Normal University, Anqing 246011, People's Republic of China
[2]School of Physics and Electrical Engineering, Anqing Normal University, Anqing 246011, People's Republic of China
[3]State Key Laboratory of Materials-Oriented Chemical Engineering and College of Chemistry and Molecular Engineering, Nanjing Tech University, Nanjing 210009, People's Republic of China

Abstract—The construction of organic-inorganic hybrid ferroelectric materials with larger, high-polarity guest molecules intercalated in kaolinite (K) faces difficulties in terms of synthesis and uncertainty of structure-property relationships. The purpose of the present study was to optimize the synthesis method and to determine the mechanism of ferroelectric behavior of kaolinite intercalated with *p*-aminobenzamide (PABA), with an eye to improving the design of intercalation methods and better utilization of clay-based ferroelectric materials. The K-PABA intercalation compound (chemical formula $Al_2Si_2O_5(OH)_4{\cdot}(PABA)_{0.7}$) was synthesized in an autoclave and then characterized using X-ray diffraction (XRD), infrared spectroscopy (IR), thermogravimetric analysis (TGA), and scanning electron microscopy (SEM). The experimental results showed that PABA expanded the kaolinite interlayer from 7.2 Å to 14.5 Å, and the orientation of the PABA molecule was ~70° from the plane of the kaolinite layers. The amino group of the PABA molecule was close to the Si sheet. The presence of intermolecular hydrogen bonds between kaolinite and PABA and among PABA molecules caused macro polarization of K-PABA and dipole inversion under the external electric field, resulting in K-PABA ferroelectricity. Simulation calculations using the Cambridge Sequential Total Energy Package (*CASTEP*) and the ferroelectricity test revealed the optimized intercalation model and possible ferroelectric mechanism.

Keywords—Ferroelectricity · Intercalate · Kaolinite · *p*-Aminobenzamide · Structure

INTRODUCTION

Ferroelectric material can reveal the switching of electric polarization, and exhibit many excellent characteristics, such as pyroelectricity, piezoelectricity, optical nonlinearities, and the electro-optic effect. Since ferroelectricity was discovered in Rochelle salt ($NaKC_4H_4O_6{\cdot}4H_2O$) (Valasek 1921), ferroelectric material has always been an important topic in condensed matter science, and the application is important as a basic element of devices and memories (Lines & Glass 2001). Recently, much attention has been focused on developing inorganic-organic hybrid ferroelectric materials (Guloy et al. 2001; Zhao et al. 2009; Chen et al. 2015; Huang et al. 2017; Xu et al. 2017; Ji et al. 2018) because of the advantages of combining an inorganic unit (rigid, dimensional stability, and thermal stability) with organic components (straightforward synthesis approach, easily tailored molecular structure, and functional properties). The technologically useful ferroelectricity requires that the compound crystallizes only in a polar space group. Over the past decades, supramolecular chemistry and crystal engineering strategies have exhibited remarkable capabilities in self-assembly of designed functional materials (Lehn 1985; Desiraju & Parshall 1989; Fabbrizzi & Poggi 1995; Braga & Grepioni 1999; Guloy et al. 2001; Desiraju 2007; Radhakrishnan 2008).

As a natural clay mineral, kaolinite (K, chemical formula $Al_2Si_2O_5(OH)_4$) with a typical 1:1 dioctahedral layered structure (Murray & Keller 1993) forms an excellent host material. The layers are stacked along the *c* axis via hydrogen bonds and dipolar interactions, and due to attractive Van der Waals forces. The polar interlayer space can accommodate guest molecules to form intercalation compounds. Due to the tight bonding between the kaolinite layers, only a few small molecules with high polarity can be intercalated directly into kaolinite. These include dimethyl sulfoxide (DMSO) (Fafard et al. 2017), potassium acetate (KAc) (Kristof et al. 1993; Yariv et al. 2000; Frost et al. 2001), hydrazine (Barrios 1977; Frost et al. 1999; Cruz & Franco 2000), formamide (Adams et al. 1976; Theng 1984), phenylphosphonic acid (Breen et al. 2002), and urea (Seifi et al. 2016; Zhang et al. 2016), whereas most other functional guests are usually indirectly intercalated by replacing previously intercalated molecules, which limits the application of kaolinite intercalation compounds in environmental protection (He et al. 2001), polymer-clay nanocomposites (Liu 2007; Letaief & Detellier 2009; Matusik et al. 2011), electrochemistry (Braggs et al. 1994; Letaief et al. 2008; Dedzo et al. 2012), catalysis (Nakagaki et al. 2004; Ayodele & Hameed

Electronic supplementary material The online version of this article (https://doi.org/10.1007/s42860-019-00036-x) contains supplementary material, which is available to authorized users.

* E-mail address of corresponding author: zsp200109@163.com
DOI: 10.1007/s42860-019-00036-x

2013), pharmaceuticals (Carretero & Pozo 2009), ionic liquids (Letaief & Detellier 2009; Dedzo & Detellier 2013), and dielectrics (Orzechowski et al. 2006; Wang et al. 2018), etc. The ferroelectricity of kaolinite intercalation compounds, however, has received much less attention. Using Grand canonical Monte Carlo simulations, Croteau et al. (2010) investigated the structure of water adsorbed on kaolinite surfaces with trenchlike defects, which indicated that kaolinite has unique advantages in the construction of inorganic-organic hybrid ferroelectrics. Others (Zhao et al. 2012; Qiao et al. 2017) reported that kaolinite intercalated with selected small molecules (DMSO, urea, and ethylene glycol) exhibited ferroelectricity. Consequently, insofar as crystal-oriented synthesis of kaolinite-based inorganic-organic hybrid ferroelectrics is concerned, a feasible strategy for achieving polar hybrid crystals is to select or design suitable organic guest molecules to intercalate kaolinite.

In the present study, PABA was selected as the candidate for intercalation for two reasons: (1) PABA with an acceptor amide group on the first carbon atom of the benzene and a donor amino group on the fourth carbon atom (Fig. 1) has high polarity, so the formation of an intercalation compound is possible through hydrogen bonds interacting with SiO_4 or hydroxyl groups (Al-OH) on the inner surface of kaolinite layers. (2) PABA can provide maximum acentricity for the molecule and give rise to a non-centrosymmetric crystal structure (Almeida et al. 2013) due to the aforementioned special structure, thus the intercalation compound is more likely to crystallize in a polar space group, which is favorable for the construction of hybrid ferroelectrics with large polarity. However, negative factors still exist: firstly, PABA has a high melting point (182–184°C) and a larger molecular size than DMSO and urea, so kaolinite intercalation is difficult to achieve using traditional methods (melting or mechanical stirring for a long time); secondly, direct observation of the binding mode between PABA and kaolinite is difficult, which means the mechanism by which ferroelectricity is achieved is unclear. In contrast, the autoclave method is suitable for higher-temperature synthesis reaction, because of the advantages of the lack of requirement for stirring and a definite pressure being exerted to facilitate the intercalation, so the above problems of synthesis can be solved easily. At the same time, theoretical calculations can be used in the design of new materials by simulating the bonding mode between guest molecules and the kaolinite layer, by supplementing the information obtained from chemical experiments, and by predicting ferroelectricity of the intercalation compound that have not been observed so far. The purpose of the present study was to test the autoclave method for preparing K-PABA and to characterize the resulting intercalated structure and explain a possible mechanism for its ferroelectric properties.

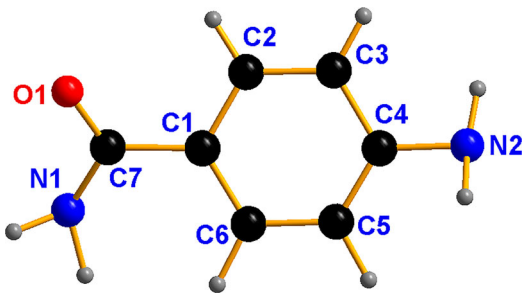

Fig. 1 Schematic diagram of the crystal structure of the PABA molecule drawn according to cif file (Alléaume 1967; Berkovitch-Yellin et al. 1985).

EXPERIMENTAL

Materials

The kaolinite sample (KGa-1b) was obtained from the Source Clays Repository of The Clay Minerals Society. It has an average particle size of 1250 mesh, contains some Fe_2O_3 (≤0.03 wt.%), Al_2O_3 (36±0.5 wt.%), and SiO_2 (47±0.5 wt.%). Analytical grade DMSO and PABA purchased from Aladdin Reagent Co., Ltd. (Shanghai, China) were used without further purification, and all operations were carried out in air.

Preparation of K-PABA Intercalation Compound

The K-PABA intercalation compound was prepared in an autoclave by replacing a DMSO precursor. The K-DMSO precursor was prepared first according to the disclosed procedure (Takenawa et al. 2001). Secondly, PABA (1.0 g) and K-DMSO (1.0 g) were sealed in a 25 mL autoclave for heating at 180°C for 12 h and then cooled to ambient temperature. 30 mL of hot ethanol was added and then the sample was stirred for 10 min, separated by a Buchner funnel suction filter (100 mm diameter membrane) to remove adsorbed guest molecules, and then the solid powder was dried at 60°C for >24 h.

In addition, to achieve the optimum preparation conditions of K-PABA, a series of K-PABA samples was synthesized at various preparation temperatures (from 150 to 200°C) and times (from 7 to 17 h at 180°C), and the relationship between the rate of intercalation (I.R.) and preparation conditions was investigated in detail.

Characterization

X-ray diffraction (XRD) patterns of kaolinite and the intercalated samples were measured using a Bruker D8 Advance Diffractometer (Bruker AXS, Rheinstetten, Baden-Wuerttemberg, Germany) with CuKα radiation (λ = 1.5418 Å) at ambient temperature. Fourier-transform Infrared spectroscopy (FTIR) was carried out using a Nicolet AVATAR-360 spectrometer (Nicolet Instrument Corp., Madison, Wisconsin, USA) (KBr disks, 4000–400 cm^{-1}). Thermogravimetric (TG) analysis was performed using a simultaneous SDT 2960 DTA-TG (TA instrument, Inc., New Castle, Delaware, USA); the sample was held in a Pt pan under a N_2 flow rate of 100 mL min^{-1} and heated at a ramping rate of 10°C·min^{-1} from ambient temperature to 700°C. The morphology of the samples was investigated using

https://doi.org/10.1007/s42860-019-00036-x Published online by Cambridge University Press

an Hitachi S-4800 scanning electron microscope (SEM) (Hitachi High-Technologies Corp., Tokyo, Japan). The polarization–electric field (*P-E*) hysteresis loops for the powdered samples were performed using a Precision Multi-ferroeletric tester (Radiant Technologies, Inc. Albuquerque, New Mexico, USA) in an AC electric field, the powdered samples were pressed into pellets at 10 MPa for 1 min with a thickness of ~0.359 mm and an area of 132.67 mm^2, and each pellet was sandwiched by copper electrodes and immersed in insulating oil while being measured.

Computational Details

The primitive unit cell of kaolinite is known as a = 5.15 Å, b = 8.94 Å, c = 7.39 Å, and α = 91.93°, β = 105.04°, γ = 89.79°, then one supercell was built with the basal spacing of layers set to 14.5 Å obtained from the XRD measurements. The possible structural models of K-PABA were calculated using the quantum mechanical program *CASTEP* (Segall et al. 2002; Clark et al. 2005) with the GGA-PW91 (generalized gradient approximation-Perdew-Wang 91) function (Perdew et al. 1996), which is appropriate for the relatively weak interactions (Martorell et al. 2010). The cutoff energy based on the plane wave was set at 300 eV for K-PABA. The convergence parameters were set as follows: self-consistent field (SCF) tolerance, 1×10^{-6} eV per atom; total energy tolerance, 1×10^{-5} eV per atom; maximum force tolerance, 0.03 eV $Å^{-1}$; maximum stress component, 0.05 GPa; and displacement of convergence tolerance, 0.001 Å. The other calculation parameters were set at the default values in the *CASTEP* code. All the aforementioned limits were able to constrain accurately the simulative process to end with a stable construction of K-PABA.

RESULTS AND DISCUSSION

XRD Analysis

The XRD pattern (Fig. 2a) displayed the 001 reflection at 7.2 Å (12.12°2θ) of pure kaolinite. A new, sharp, high-intensity peak appeared in K-DMSO with a d_{001} value of 11.2 Å (7.94°2θ), which represents a lattice expansion of 4.0 Å relative to pure kaolinite. The PABA-intercalated kaolinite obtained from K-DMSO was a white powder with a basal lattice spacing of 14.5 Å (6.12°2θ), which represents a lattice expansion of 7.3 Å in relation to pure kaolinite. In this case, the

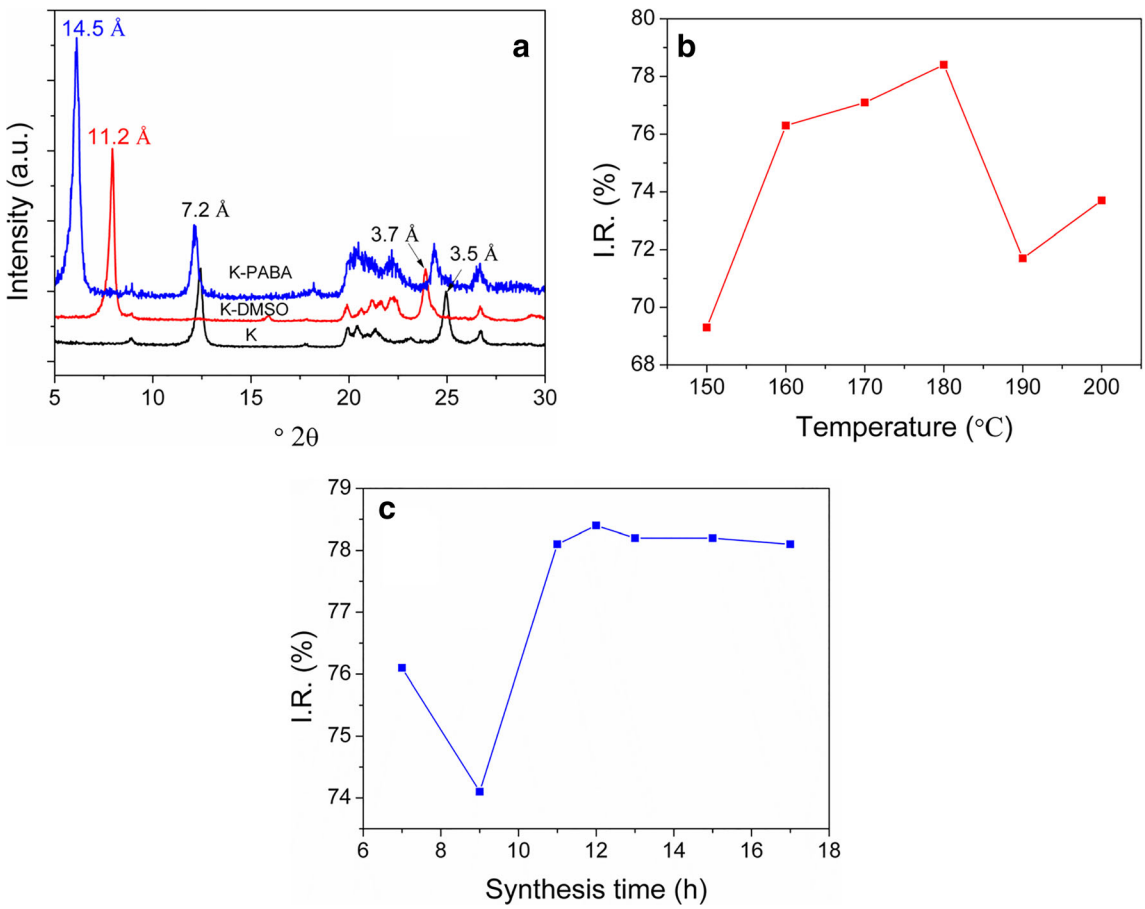

Fig. 2 XRD patterns (5–30°2θ) of (**a**) K, K-DMSO, and K-PABA at 180°C, (**b**) plot of the K-PABA intercalation rate (I.R.) versus synthesis temperature (150–200°C), (**c**) plot of the K-PABA intercalation rate (I.R.) versus synthesis time (7–17 h at 180°C).

https://doi.org/10.1007/s42860-019-00036-x Published online by Cambridge University Press

I.R. can be calculated directly as 78.4% based on the change of diffraction peak intensity before and after intercalation (Ledoux & White 1964). Meanwhile, the XRD pattern (Fig. 2a) showed no evidence of a DMSO residue in the K-PABA, implying that the substitution of PABA was completed and that the only crystalline materials observed within the matrix were kaolinite and the expected K-PABA intercalated composite. In addition, based on the plots of intercalation rate versus temperature and time (Fig. 2b and c), the ideal condition for K-PABA synthesis was 180°C for 12 h.

FTIR Analysis

FTIR measurements (Fig. 3) revealed three characteristic bands for kaolinite at 3695, 3662, and 3652 cm^{-1}, being ascribed to weak, acid-active, inner-surface hydroxyl groups (inner-surface OH) and a sharp peak at 3620 cm^{-1}, being assigned to an inner hydroxyl band (inner OH) (Balan et al. 2010). K-DMSO produced two bands at 3695 and 3620 cm^{-1} similar to pure kaolinite, while the band at 3652 cm^{-1} disappeared and that at 3662 cm^{-1} became sharper, suggesting the formation of hydrogen bonds between inner-surface OH and the Si=O group of the DMSO. Slightly stronger new bands were observed at 3536 and 3500 cm^{-1}, suggesting that the inner surface OH bands were disturbed by intercalation molecules. In addition, K-DMSO also had two weak, broad bands at 3023 and 2937 cm^{-1}; while liquid DMSO appeared at 2994 and 2911 cm^{-1}, which is related to the symmetric stretching of $–CH_3$ in DMSO.

In contrast, only two sharper characteristic OH bands of kaolinite were observed at 3695 and 3620 cm^{-1} in K-PABA, as well as a band at 3500 cm^{-1} and a new shoulder peak at 3635 cm^{-1}, indicating that PABA successfully replaced DMSO and formed hydrogen bonds with kaolinite layers. Bands at 3481 cm^{-1} and 3468 cm^{-1} correspond to the stretching vibration of N–H of PABA. A strong, sharp peak at 3408 cm^{-1} and two broad bands at 3357 cm^{-1} and 3224 cm^{-1} indicate the associations existing between guest molecules, similar to that observed for pure PABA molecules at 3326 cm^{-1} and 3323 cm^{-1}. In addition, the stretching vibration bands of the aromatic ring skeleton (Gardolinski et al. 2000) were observed in the range 1606–1443 cm^{-1}, while a band at 840 cm^{-1} confirmed the guest molecule was a *para*-disubstituted compound on the benzene ring. The band at ~1630 cm^{-1} was attributed to the overlap of N–H bending and C=O stretching vibrations, which moved ~20 cm^{-1} toward the low-wavenumber region compared with C=O of the free amide group, indicating that C=O of the amide group in the guest molecule also formed hydrogen bonds. Therefore, some conclusions can be drawn: K-PABA was prepared successfully, which was consistent with the XRD results, and both C=O and N–H from PABA molecules participated in the formation of hydrogen bonds. However, whether N–H comes from the amino or amide group needs further research.

TG Analysis

The TG curves for the pure kaolinite (Fig. 4) showed a mass-loss step (at ~500°C) related to the thermal dehydroxylation of kaolinite into meta-kaolinite. For K-DMSO, the initial decrease in the mass was probably related to the removal of adsorbed water, but the intense decrease in mass (~13%) between 100 and 207°C was associated with the removal of DMSO molecules. The jump at ~500°C was similar to that observed in pure kaolinite. The TG curve for K-PABA proved that heating at 207°C decreased the mass of the sample by 21.19% and then, after heating at 344°C, to a relative decrease of 11.46%. The 21.19% decrease was assigned to deintercalation and decomposition of PABA molecules, indicating that the kaolinite inorganic layers improved the thermal stability of PABA (Prasad et al. 2011). The second decrease (at ~344–620°C) was interpreted as a dehydroxylation of kaolinite similar to pure kaolinite. This process generated a mass loss of 11.46%, similar to the 13.9% value predicted from the theoretical formula of pure kaolinite ($Al_2Si_2O_5(OH)_4$) (Kristof

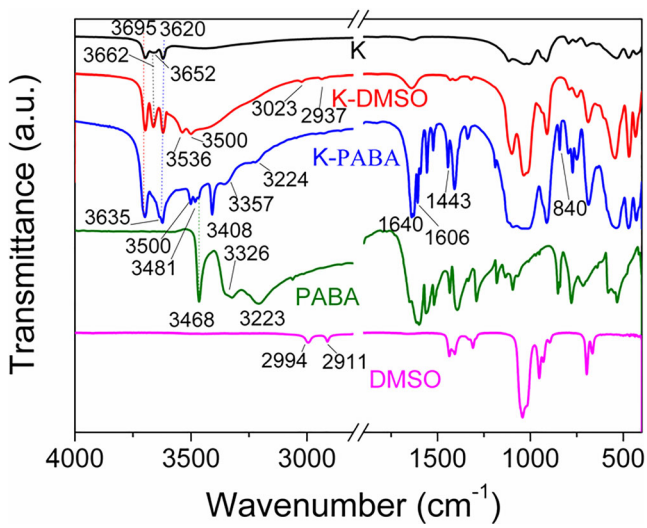

Fig. 3 FTIR of liquid DMSO, pure PABA, K, K-DMSO, and K-PABA in the wavenumber range 4000–400 cm^{-1}.

https://doi.org/10.1007/s42860-019-00036-x Published online by Cambridge University Press

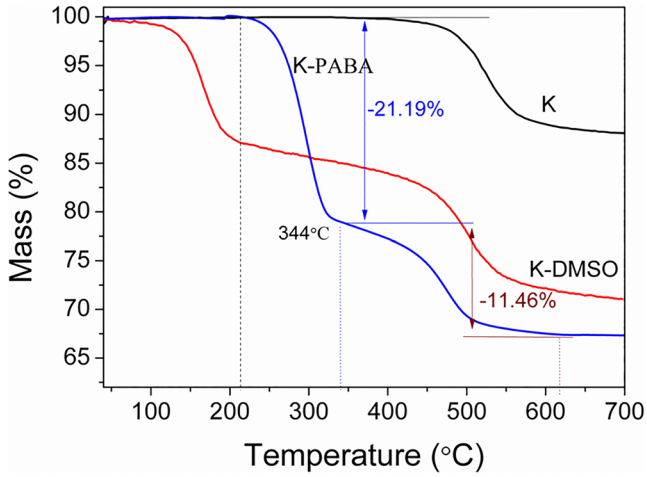

Fig. 4 TG curves of K, K-DMSO, and K- PABA.

et al. 1999). Finally, the chemical formula of K-PABA can be expressed as $Al_2Si_2O_5(OH)_4{\cdot}(PABA)_{0.7}$ on the basis of mass loss (21.19%) and intercalation rate (78.4%).

SEM Analysis

The SEM image of pure kaolinite morphology (Fig. 5a) revealed a well ordered stack with a tightly layered structure. The morphology of K-DMSO is almost the same as pure kaolinite (Fig. 5b), indicating that K-DMSO still has a long-range ordered structure. In contrast, the images for K-PABA (Fig. 5c, d) showed small stacks and some individual, thin flakes related to exfoliation or a departure from a layered structure, confirming that the long-range order of kaolinite was destroyed but the short-range order remained. The SEM results are direct evidence that the kaolinite layered structure was changed by PABA intercalation.

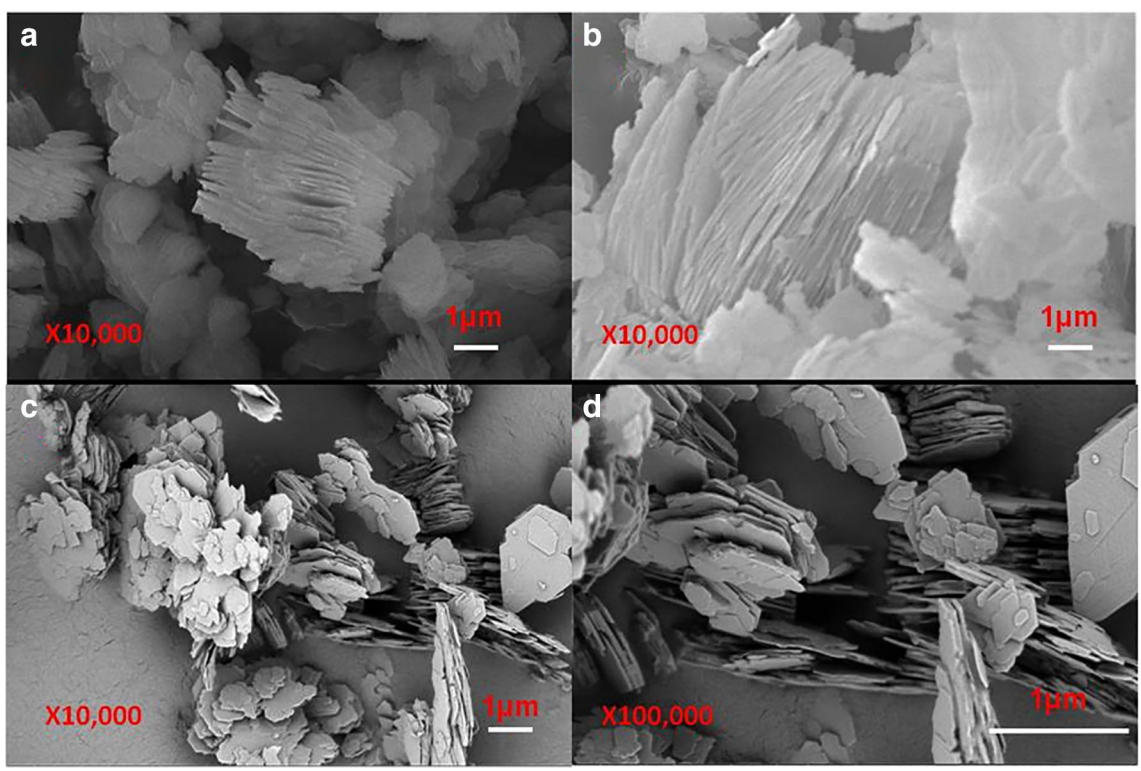

Fig. 5 SEM images of (**a**) K, (**b**) K-DMSO, and (**c** and **d**) K-PABA.

https://doi.org/10.1007/s42860-019-00036-x Published online by Cambridge University Press

Structural Optimization

From the calculated chemical formula $Al_2Si_2O_5(OH)_4{\cdot}(PABA)_{0.7}$ of K-PABA, each unit cell contains a PABA molecule. The molecular dimension of PABA, measured between the *p*-substituted amino group hydrogen and the hydrogen atom of the amide group was determined to be ~7.9 Å (Fig. S3) using *Material Studio 6.0* software. Therefore, based on the variations in the 7.3 Å interlayer spacing of the kaolinite after intercalation, each intercalated molecule was oriented at an angle of ~70° to the plane of the kaolinite layer. In fact, this conclusion agrees with the 50–75° orientation angle that is normally assumed by hydroxyl groups at the surface of the kaolinite layer (Olejnik et al. 1968; Gardolinski et al. 2000; Kloprogge 2019). Moreover, two orientations of PABA are possible between kaolinite layers because amide and amino groups on benzene rings have the ability to form hydrogen bonds with the kaolinite layer. In the structural optimizations (Fig. 6), the amino group close to the Si-sheet was labeled model A and that near the Al-sheet was marked as model B (Fig. S2). In the process of geometric optimization of K-PABA performed using the *CASTEP* module, all the atoms and unit-cell parameters (*a*, *b*, α, β, and γ) were relaxed, but the *c*-axis length was fixed at 14.5 Å.

Both optimization models (A and B) (Table S1) yielded similar crystal structure parameters. The remarkable difference was that the calculated final energy of model A was 166.6 kJ/mol less than model B, which suggested that model A was more reasonable. The rationality of model A can be confirmed further by simulating XRD (Fig. S1), where the position of the 001 peak in the simulated (6.12°2θ) patterns deviated from the experimental ones (6.12°2θ) by <1%.

The structural parameters of optimized and crystalline PABA are given in Table S2. Some optimized bonds (C7–O1, C7–N1, and C4–N2) were longer than those in the crystalline state. In addition, angle 1 became larger and angle 2 became smaller, indicating that the guest molecule was subjected to a force in the direction of the *c* axis of kaolinite. This force was ascribed to the hydrogen-bond interactions between kaolinite and PABA. On the other hand, torsion angles observed in both states indicated that the benzene ring of PABA was not coplanar with two substituent groups, suggesting amino and amide groups were affected by different forces. The resulting differences of torsion angles provide strong evidence that PABA in K-PABA was also affected by inorganic laminates, except for the intermolecular interactions of organic parts similar to those in the crystal state; in other words, strong hydrogen bond interactions exist between kaolinite and PABA, as well as between PABA molecules, indicating that both amino and amide groups participate in the interaction process.

With respect to H···Y hydrogen-bond studies, the bond distance was limited to <3.2 Å and a minimum value for the X-H···Y angle was set as 90° (Schuster et al. 1976; Jeffrey 1997; Steiner 2002; Desiraju & Steiner 2001; Benco et al. 2001). Notable hydrogen bonds were observed in model A in three places: (1) inside kaolinite laminates, including the Al-sheet and Si-sheet; (2) between PABA and kaolinite layers (PABA-kaolinite), such as N2–H···$O_{(Al\text{-}sheet)}$, N1···H–$O_{(Si\text{-}sheet)}$, and O1···H–$O_{(Si\text{-}sheet)}$; and (3) between PABA molecules (PABA-PABA), i.e. O1···H–N1 (3*a* = 2.185 Å, 3*b* = 2.996 Å) of amide groups formed an infinite one-dimensional chain along the *a* axis. Apparently, the hydrogen bonds of (1) were responsible for the stability

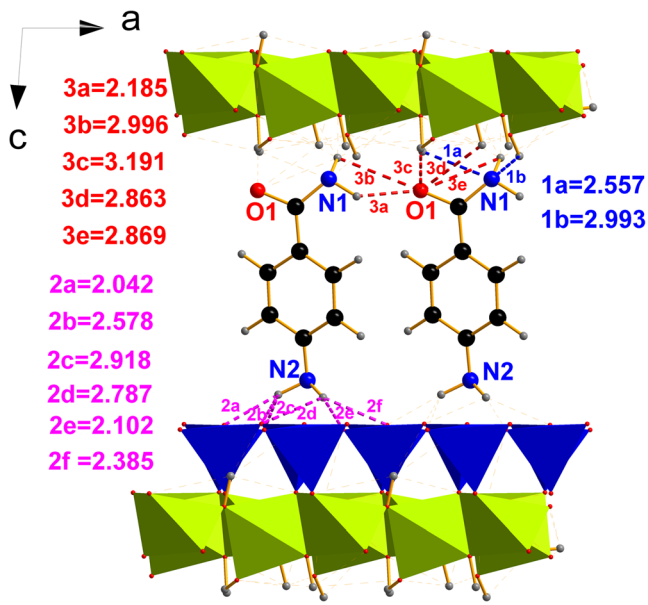

Fig. 6 The optimized structural model A (amino groups close to the Si-sheet) of K-PABA viewed along the *b* axis. Various hydrogen bonds were marked on the graph, where 1 and 2 refer, respectively, to intermolecular hydrogen bonds formed by amino groups with kaolinite and amide groups with kaolinite, while 3 refers to intermolecular hydrogen bonds between PABA molecules.

https://doi.org/10.1007/s42860-019-00036-x Published online by Cambridge University Press

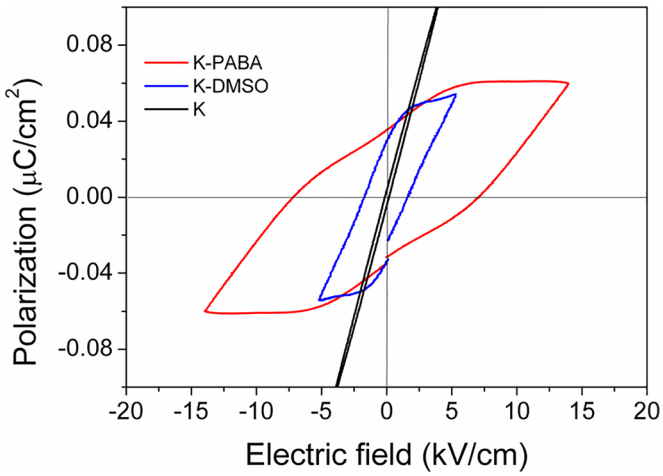

Fig. 7 The polarization–electric field (P-E) hysteresis loops of K, K-DMSO, and KPABA measured at room temperature.

of the inorganic layer. The latter two in (2) and (3) played an important role in the formation of K-PABA. As a consequence, the guest molecules were actually inclined between kaolinite layers, and formed an infinite two-dimensional network on the *ac* plane through the aforementioned two intermolecular hydrogen bonds, further revealing that an amide group is involved in the formation of hydrogen bonds of PABA-kaolinite and PABA-PABA, while the amino group only participates in that of PABA-kaolinite.

Ferroelectricity

A hysteresis loop is one of the prominent characteristics of ferroelectric materials, which usually means that the sample contains some macroscopic polarizations, and the macroscopic polarization axis can be reversed under the action of an external electric field. The polarization–electric field (P-E) measurements (Fig. 7) displayed a hysteresis loop of K-PABA powder at room temperature, 14 kV/cm electric field, and 10 Hz frequency, at which the saturation polarization strength (P_s), residual polarization strength (P_r), and coercive field (E_c) were 0.06 μC/cm^2, 0.0352 μC/cm^2, and 7.1 kV/cm, respectively. In contrast, pure kaolinite exhibits a linear hysteresis loop suggesting no ferroelectricity; while K-DMSO has a hysteresis loop (Zhao et al. 2012), but the E_c of K-PABA is significantly larger, probably due to the larger size of the PABA molecule. In addition, the P_s of K-

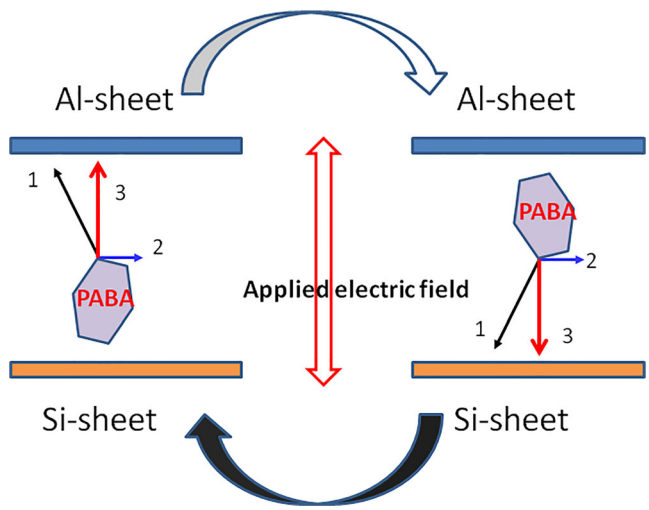

Fig. 8 Schematic illustrations of possible dipole reversal in the PABA molecules by exposure to an applied AC electric field in the K-PABA sample. Arrows 1 and 2 indicate the intermolecular hydrogen bonds formed in PABA-kaolinite and PABA-PABA, respectively, while arrow 3 refers to the dipole of the whole K-PABA.

https://doi.org/10.1007/s42860-019-00036-x Published online by Cambridge University Press

PABA is smaller than that of a typical ferroelectric crystal $BaTiO_3$ (Xiong et al. 2014).

Free PABA with high polarity has a permanent dipole along the axis from the amino group to the amide group, and this dipole becomes tilted at an angle of ~70° relative to the plane of the kaolinite layer in K-PABA, as shown by arrow 1 in Fig. 8. Arrow 2 refers to the dipole of intermolecular hydrogen bonds between PABA molecules on the *a* axis, so the macroscopic polarization axis of the whole K-PABA should be almost parallel to the *c* axis of kaolinite as indicated by arrow 3. In fact, the intermolecular hydrogen bond energy is usually ~10–65 kJ/mol (Horiuchi & Tokura 2008; Szafrański & Katrusiak 2008), which is relatively easily destroyed by an external electrics (Williams & Moore 1972; Ye et al. 2008; Cornelissen et al. 2019). On the other hand, the unit-cell volumes of K-PABA and kaolinite are known to be 756.19 $Å^3$ and 327.84 $Å^3$, respectively; thus the interlayer space of the intercalated compound is 428.35 $Å^3$ (ΔV = 751.19 – 327.84 $Å^3$), which is greater than the 167.54 $Å^3$ of each PABA volume (molecular unit-cell volume is 335.08 $Å^3$, Z = 2) (Alléaume 1967; Berkovitch-Yellin et al. 1985). This implied that the kaolinite interlayer can provide a space for PABA to move, although the guest molecule cannot flip between kaolinite layers like small molecules (DMSO and urea) can, due to their large molecular size (~7.9 Å). For these reasons, when an external AC electric field was applied to K-PABA along the *c* axis, the intermolecular hydrogen bonds of PABA-kaolinite are reversed (arrow 1), while the original direction of the *a* axis was maintained (arrow 2) because it was almost perpendicular to the direction of the external electric field. As a result, the dipole of the entire K-PABA (arrow 3) was reversed under the action of the external AC electric field. Obviously, the real ferroelectric mechanism of K-PABA is more complicated than the above analysis, and further research is necessary.

CONCLUSIONS

In summary, autoclaving is an effective method to intercalate kaolinite with PABA at 180°C over 12 h. The acquisition of a K-PABA polar hybrid crystal further proved that the strategy of intercalating kaolinite with a polar guest is successful. The interlayer spacing, intercalation ratio, and mass-loss rate of K-PABA reached 14.5 Å, 78.4%, and 21.19%, respectively. Theoretical calculation disclosed correctly the arrangement of PABA between kaolinite layers. The intercalation of PABA not only changed the morphology and structure of kaolinite, but also generated the intermolecular hydrogen bonds in kaolinite-PABA and PABA-PABA, which lead to ferroelectricity of K-PABA. This work provided a useful exploration for the design and application of kaolinite hybrid ferroelectrics.

ACKNOWLEDGEMENTS

The authors gratefully acknowledge the financial support provided by the Natural Science Foundation of Anhui Education Department (No. KJ2018A0381) and the Anhui Provincial Key Laboratory of Optoelectronic and Magnetism Functional Material (ZD2017003).

REFERENCES

Adams, J. M., Reid, P. I., Thomas, J. M., & Walters, M. J. (1976). On the hydrogen atom positions in a kaolinite: formamide intercalate. *Clays and Clay Minerals, 24*, 267–269.

Alléaume, M. (1967) Etude cristallographique de composés sulfamidés. (Doctoral dissertation, Université de Bordeaux).

Almeida, A. R., Monte, M. J., Matos, M. A. R., & Morais, V. M. (2013). Experimental and computational thermodynamic study of ortho-meta-and para-aminobenzamide. *The Journal of Chemical Thermodynamics, 59*, 222–232.

Ayodele, O. B., & Hameed, B. H. (2013). Development of kaolinite supported ferric oxalate heterogeneous catalyst for degradation of 4-nitrophenol in photo-Fenton process. *Applied Clay Science, 83*, 171–181.

Balan, E., Delattre, S., Guillaumet, M., & Salje, E. K. (2010). Low-temperature infrared spectroscopic study of OH-stretching modes in kaolinite and dickite. *American Mineralogist, 95*, 1257–1266.

Barrios, J. (1977). Qualitative and quantitative study of stacking faults in a hydrazine treated kaolinite-relationship with the infrared spectra. *Clays and Clay Minerals, 25*, 422–429.

Benco, L., Tunega, D., Hafner, J., & Lischka, H. (2001). Upper limit of the O-H…O hydrogen bond. Ab initio study of the kaolinite structure. *The Journal of Physical Chemistry B, 105*, 10812–10817.

Berkovitch-Yellin, Z., Van Mil, J., Addadi, L., Idelson, M., Lahav, M., & Leiserowitz, L. (1985). Crystal morphology engineering by "tailor-made" inhibitors; a new probe to fine intermolecular interactions. *Journal of the American Chemical Society, 107*, 3111–3122.

Braga, D., & Grepioni, F. (1999). Crystal engineering: from molecules and crystals to materials. In: (D. Braga, F. Grepioni, and F. Orpen, Eds) *Crystal Engineering: From Molecules and Crystals to Materials*, Springer, Dordrecht, 421-441.

Braggs, B., Fornasiero, D., Ralston, J., & Smart, R. S. (1994). The effect of surface modification by an organosilane on the electrochemical properties of kaolinite. *Clays and Clay Minerals, 42*, 123–136.

Breen, C., D'Mello, N., & Yarwood, J. (2002). The thermal stability of mixed phenylphosphonic acid/water intercalates of kaolin and halloysite. A TG-EGA and VT-DRIFTS study. *Journal of Materials Chemistry, 12*, 273–278.

Carretero, M. I., & Pozo, M. (2009). Clay and non-clay minerals in the pharmaceutical industry: Part I. Excipients and medical applications. *Applied Clay Science, 46*, 73–80.

Chen, B., Shi, J., Zheng, X., Zhou, Y., Zhu, K., & Priya, S. (2015). Ferroelectric solar cells based on inorganic-organic hybrid perovskites. *Journal of Materials Chemistry A, 3*, 7699–7705.

Clark, S. J., Segall, M. D., Pickard, C. J., Hasnip, P. J., Probert, M. I., Refson, K., & Payne, M. C. (2005). First principles methods using CASTEP. *Zeitschrift für Kristallographie-Crystalline Materials, 220*, 567–570.

Cornelissen, T. D., Biler, M., Urbanaviciute, I., Norman, P., Linares, M., & Kemerink, M. (2019). Kinetic Monte Carlo simulations of organic ferroelectrics. *Physical Chemistry Chemical Physics, 21*, 1375–1383.

Croteau, T., Bertram, A. K., & Patey, G. N. (2010). Observations of high-density ferroelectric ordered water in kaolinite trenches using

https://doi.org/10.1007/s42860-019-00036-x Published online by Cambridge University Press

Monte Carlo simulations. *The Journal of Physical Chemistry A, 114*, 8396–8405.

Cruz, M. D. R., & Franco, F. (2000). Thermal behavior of the kaolinite-hydrazine intercalation complex. *Clays and Clay Minerals, 48*, 63–67.

Dedzo, G. K., & Detellier, C. (2013). Ionic liquid-kaolinite nanohybrid materials for the amperometric detection of trace levels of iodide. *Analyst, 138*, 767–770.

Dedzo, G. K., Letaief, S., & Detellier, C. (2012). Kaolinite-ionic liquid nanohybrid materials as electrochemical sensors for size-selective detection of anions. *Journal of Materials Chemistry, 22*, 20593–20601.

Desiraju, G. R. (2007). Crystal engineering: a holistic view. *Angewandte Chemie International Edition, 46*, 8342–8356.

Desiraju, G. R., & Parshall, G. W. (1989). Crystal engineering: the design of organic solids. *Materials Science Monographs*, *54*.

Desiraju, G. R. & Steiner, T. (2001) *The Weak Hydrogen Bond: in Structural Chemistry and Biology*. Monograph, 9, International Union of Crystallography, 507 pp.

Fabbrizzi, L., & Poggi, A. (1995). Sensors and switches from supramolecular chemistry. *Chemical Society Reviews, 24*, 197–202.

Fafard, J., Terskikh, V., & Detellier, C. (2017). Solid-state ^{1}H and ^{27}Al NMR studies of DMSO-kaolinite intercalates. *Clays and Clay Minerals, 65*, 206–219.

Frost, R. L., Kloprogge, J. T., Kristof, J., & Horvath, E. (1999). Deintercalation of hydrazine-intercalated low-defect kaolinite. *Clays and Clay Minerals, 47*, 732–741.

Frost, R. L., Kristof, J., Schmidt, J. M., & Kloprogge, J. T. (2001). Raman spectroscopy of potassium acetate-intercalated kaolinites at liquid nitrogen temperature. *Spectrochimica Acta Part A: Molecular and Biomolecular Spectroscopy, 57*, 603–609.

Gardolinski, J. E., Ramos, L. P., de Souza, G. P., & Wypych, F. (2000). Intercalation of benzamide into kaolinite. *Journal of Colloid and Interface Science, 221*, 284–290.

Guloy, A. M., Tang, Z., Miranda, P. B., & Srdanov, V. I. (2001). A new luminescent organic-inorganic hybrid compound with large optical nonlinearity. *Advanced Materials, 13*, 833–837.

He, H. P., Guo, J. G., Zhu, J. X., & Yang, D. (2001). An experimental study of adsorption capacity of montmorillonite, kaolinite and illite for heavy metals. *Acta Petrologica et Mineralogica, 4*, 574–578.

Horiuchi, S., & Tokura, Y. (2008). Organic ferroelectrics. *Nature Materials, 7*, 357–366.

Huang, B., Sun, L. Y., Wang, S. S., Zhang, J. Y., Ji, C. M., Luo, J. H., Zhang, W. X., & Chen, X. M. (2017). A near-room-temperature organic-inorganic hybrid ferroelectric: $[C_6H_5CH_2CH_2NH_3]_2[CdI_4]$. *Chemical Communications, 53*, 5764–5766.

Jeffrey, G. A. (1997). *An Introduction to Hydrogen Bonding* (Vol. 12, p. 228). New York: Oxford University Press.

Ji, C., Liu, S., Han, S., Tao, K., Sun, Z., & Luo, J. (2018). Towards a spectrally customized photoresponse from an organic-inorganic hybrid ferroelectric. *Angewandte Chemie International Edition, 57*, 16764–16767.

Kloprogge, J. T. (2019). The Kaolin Group: Hydroxyl Groups. In: *Spectroscopic Methods in the Study of Kaolin Minerals and Their Modifications*. Springer, Berlin, pp. 41–96.

Kristof, J., Frost, R., Kloprogge, J., Horváth, E., & Gábor, M. (1999). Thermal behaviour of kaolinite intercalated with formamide, dimethyl sulphoxide and hydrazine. *Journal of Thermal Analysis and Calorimetry, 56*, 885–891.

Kristof, J., Mink, J., Horvath, E., & Gábor, M. (1993). Intercalation study of clay minerals by Fourier transform infrared spectrometry. *Vibrational Spectroscopy, 5*, 61–67.

Ledoux, R. L., & White, J. L. (1964). Infrared study of the OH groups in expanded kaolinite. *Science, 143*, 244–246.

Lehn, J. M. (1985). Supramolecular chemistry: receptors, catalysts, and carriers. *Science, 227*, 849–856.

Letaief, S., & Detellier, C. (2009). Functionalization of the interlayer surfaces of kaolinite by alkylammonium groups from ionic liquids. *Clays and Clay minerals, 57*, 638–648.

Letaief, S., Tonle, I. K., Diaco, T., & Detellier, C. (2008). Nanohybrid materials from interlayer functionalization of kaolinite. Application to the electrochemical preconcentration of cyanide. *Applied Clay Science, 42*, 95–101.

Lines, M. E., & Glass, A. M. (2001) *Principles and Applications of Ferroelectrics and Related Materials*, Oxford University Press, UK.

Liu, P. (2007). Polymer modified clay minerals: A review. *Applied Clay Science, 38*, 64–76.

Martorell, B., Kremleva, A., Krüger, S., & Rösch, N. (2010). Density functional model study of uranyl adsorption on the solvated (001) surface of kaolinite. *The Journal of Physical Chemistry C, 114*, 13287–13294.

Matusik, J., Stodolak, E., & Bahranowski, K. (2011). Synthesis of polylactide/clay composites using structurally different kaolinites and kaolinite nanotubes. *Applied Clay Science, 51*, 102–109.

Murray, H.H., & Keller, W.D. (1993) Kaolins, kaolins and kaolins. Pp. 1–24 in: *Kaolin Genesis and Utilization* (H.H. Murray, W. Bundy, & C. Harvey, editors). Special Publication, 1. The Clay Minerals Society, Boulder, Colorado, USA.

Nakagaki, S., Benedito, F. L., & Wypych, F. (2004). Anionic iron (III) porphyrin immobilized on silanized kaolinite as catalyst for oxidation reactions. *Journal of Molecular Catalysis A: Chemical., 217* 121–131.

Olejnik, S., Aylmore, L. A. G., Posner, A. M., & Quirk, J. P. (1968). Infrared spectra of kaolin mineral-dimethyl sulfoxide complexes. *The Journal of Physical Chemistry, 72*, 241–249.

Orzechowski, K., Słonka, T., & Głowinski, J. (2006). Dielectric properties of intercalated kaolinite. *Journal of Physics and Chemistry of Solids, 67*, 915–919.

Perdew, J. P., Burke, K., & Ernzerhof, M. (1996). Generalized gradient approximation made simple. *Physical Review Letters, 77*, 3865.

Prasad, L. G., Krishnakumar, V., Nagalakshmi, R., & Manohar, S. (2011). Physicochemical properties of highly efficient organic NLO crystal: 4-Aminobenzamide. *Materials Chemistry and Physics, 128*, 90–95.

Qiao, Q., Ding, Y. N., Zhao, S. P., Li, L., Liu, J. L., & Ren, X. M. (2017). Design and preparation of a hybrid ferroelectric material through ethylene glycol covalently grafted to Kaolinite. *Inorganic Chemistry Frontiers, 4*, 1405–1412.

Radhakrishnan, T. P. (2008). Molecular structure, symmetry, & shape as design elements in the fabrication of molecular crystals for second harmonic generation and the role of molecules-in-materials. *Accounts of Chemical Research, 41*, 367–376.

Schuster, P., Zundel, G., & Sandorfy, C. (1976) *Hydrogen Bond; Recent Developments in Theory and Experiments.* North-Holland Publishing Company, Amsterdam, The Netherlands.

Segall, M. D., Lindan, P. J., Probert, M. A., Pickard, C. J., Hasnip, P. J., Clark, S. J., & Payne, M. C. (2002). First-principles simulation: ideas, illustrations and the CASTEP code. *Journal of Physics: Condensed Matter, 14*, 2717.

Seifi, S., Diatta-Dieme, M. T., Blanchart, P., Lecomte-Nana, G. L., Kobor, D., & Petit, S. (2016). Kaolin intercalated by urea. Ceramic applications. *Construction and Building Materials, 113*, 579–585.

Steiner, T. (2002). The hydrogen bond in the solid state. *Angewandte Chemie International Edition, 41*, 48–76.

Szafrański, M., & Katrusiak, A. (2008). Giant dielectric anisotropy and relaxor ferroelectricity induced by proton transfers in $NH^{+}\cdots$N-bonded supramolecular aggregates. *The Journal of Physical Chemistry B, 112*, 6779–6785.

Takenawa, R., Komori, Y., Hayashi, S., Kawamata, J., & Kuroda, K. (2001). Intercalation of nitroanilines into kaolinite and second harmonic generation. *Chemistry of Materials, 13*, 3741–3746.

Theng, B. (1984). Intercalation method using formamide for differentiating halloysite from kaolinite. *Clays and Clay Minerals, 32*, 241–248.

Valasek, J. (1921). Piezo-electric and allied phenomena in Rochelle salt[J]. *Physical Review, 17*, 475–481.

Wang, Y., Zhou, S., & Du, H. (2018). Investigation of dielectric properties of polymer composites with kaolin. *Journal of Materials Science: Materials in Electronics, 29*, 12360–12365.

Williams, H. C. W. L., & Moore, M. A. (1972). Theory of hydrogen-bonded ferroelectrics: I. *Journal of Physics C: Solid State Physics, 5*, 3168.

Xiong, C., Pernice, W. H., Ngai, J. H., Reiner, J. W., Kumah, D., Walker, F. J., & Tang, H. X. (2014). Active silicon integrated nanophotonics: ferroelectric $BaTiO_3$ devices. *Nano Letters, 14*, 1419–1425.

Xu, C., Zhang, W., Gao, L., Gan, X., Sun, X., Cui, Z., Zepeng, C., Cai, H., & Wu, X. S. (2017). A high-temperature organic-inorganic ferroelectric with outstanding switchable dielectric characteristics. *RSC Advances, 7*, 47933–47937.

Yariv, S., Lapides, I., Nasser, A., Lahav, N., Brodsky, I., & Michaelian, K. H. (2000). Infrared study of the intercalation of potassium halides in kaolinite. *Clays and Clay Minerals, 48*, 10–18.

Ye, H. Y., Fu, D. W., Zhang, Y., Zhang, W., Xiong, R. G., & Huang, S. D. (2008). Hydrogen-bonded ferroelectrics based on metal-organic coordination. *Journal of the American Chemical Society, 131*, 42–43.

Zhang, S., Liu, Q., Gao, F., Li, X., Liu, C., Li, H., Boyd, S. A., Johnston, C. T., & Teppen, B. J. (2016). Mechanism associated with kaolinite intercalation with urea: combination of infrared spectroscopy and molecular dynamics simulation studies. *The Journal of Physical Chemistry C, 121*, 402–409.

Zhao, H. R., Li, D. P., Ren, X. M., Song, Y., & Jin, W. Q. (2009). Larger spontaneous polarization ferroelectric inorganic-organic hybrids:$[PbI_3]_\infty$ chains directed organic cations aggregation to Kagomé-shaped tubular architecture. *Journal of the American Chemical Society, 132*, 18–19.

Zhao, S. P., Gao, H., Ren, X. M., Yuan, G. J., & Lu, Y. N. (2012). A facile and efficient strategy for the design of ferroelectric and giant dielectric hybrids via intercalating polar molecules into noncentrosymmetric layered inorganic compounds. *Journal of Materials Chemistry, 22*, 447–453.

(Received 31 January 2019; revised 13 September 2019; AE: Xiandong Liu)